The Effects of Three-Body Scattering on Differential Reflectivity Signatures

J. C. HUBBERT AND V. N. BRINGI

Colorado State University, Fort Collins, Colorado

(Manuscript received 18 September 1998, in final form 5 March 1999)

ABSTRACT

Effects of three-body scattering on reflectivity signatures at S and C bands can be seen on the back side of large reflectivity storm cores that contain hail. The fingerlike protrusions of elevated reflectivity have been termed flare echoes or ''hail spikes.'' Three-body scattering occurs when radiation from the radar scattered toward the ground is scattered back to hydrometeors, which then scatter some of the radiation back to the radar. Three-body scatter typically causes differential reflectivity to be very high at high elevations and to be negative at lower elevations at the rear of the storm core. This paper describes a model that can simulate the essential features of the three-body scattering that has been observed in hailstorms. The model also shows that three-body scatter can significantly affect the polarimetric Z_{DR} (differential reflectivity) radar signatures in hailshafts at very low elevation and thus is a possible explanation of the frequently reported negative Z_{DR} signatures in hailshafts near ground.

1. Introduction

Under most circumstances multiple scattering effects are considered to be negligible in radar meteorology. However, one situation where the effects of multiple scattering have been observed is in reflectivity signatures on the back side (away from the radar) of high-reflectivity cores ($Z_h > \approx 55$ dBZ) that contain hail. Fingerlike protrusions of elevated reflectivity have been observed, which are termed flare echoes or ''hail spikes.'' This type of multiple scattering is termed three-body scattering (Zrnić 1987) because of the theorized scattering path: transmitted energy is scattered to ground by the illuminated hailstones, the ground then scatters the energy back toward the main beam where hailstones again scatter some of the energy back toward the radar. Zrnić (1987) modeled three-body scattering via a modified radar equation and was able to predict the decay in intensity of the the flare echo with respect to increased range. Shown in Fig. 1 is an example of three-body scattering from DLR's (German Aerospace Agency) C-band (wavelength of about 5 cm) radar located at Oberpfaffenhofen, Germany. The top panel shows reflectivity with peak values exceeding 65 dBZ. The three-body flare echo is evident on the right side of the panel; that is, the direct backscatter for ranges greater than about 90 km is very small so that the seen reflectivity contours are probably due exclusively to three-body scatter. The lower panel shows the associated Z_{DR} (differential reflectivity) field. In the area of three-body scattering, the -1- to 1-dB contour of Z_{DR} forms roughly a 45° angle with the ground. This contour area separates, in general, positive Z_{DR} values (above) from the negative values (below). This pattern in Z_{DR} is seen quite frequently in flare echoes in DLR and in Colorado State University (CSU)–CHILL (S band, wavelength of about 11 cm) radar data, though it is typically much more pronounced at C band. Note the extrema of $Z_{DR} > +9$ dB and $Z_{DR} < -5$ dB, which would be difficult to explain microphysically. The expected value of Z_{DR} in this low reflectivity area is 0 dB, which is observed in very light rain or in randomly oriented ice particles.

Thus far in the literature, reported three-body scattering observations has been limited to flare echos found on the back side of high reflectivity cores. In this paper, the possible effects of three-body scattering contaminating the main signal in storm cores is also considered. We hypothesize that another possible artifact of three-body scattering in Z_{DR} is seen underneath the storm core at ranges from 79 to 88 km, where Z_{DR} is quite negative with some values less than -3 dB. Researchers have explained these negative values microphysically; that is, hail of certain size and shape were assumed to be responsible (Bringi et al. 1984; Zrnić et al. 1993). Model studies at S band show that vertically oriented conical hail less than about 4 cm (Aydin et al. 1984), vertically oriented oblate hail less than about 4 cm, and horizontally oriented oblate hail greater than about 4 cm (Aydin and Zhao 1990) can produce such Z_{DR} signatures. However, it has not been shown that hailstones actually do fall in such an orientation to cause Z_{DR} to be negative.

Corresponding author address: Dr. John Hubbert, Dept. of Electrical Engineering, Colorado State University, Fort Collins, CO 80523-1373.
E-mail: hubbert@engr.colostate.edu

© 2000 American Meteorological Society

Unauthenticated | Downloaded 04/13/21 05:55 AM UTC

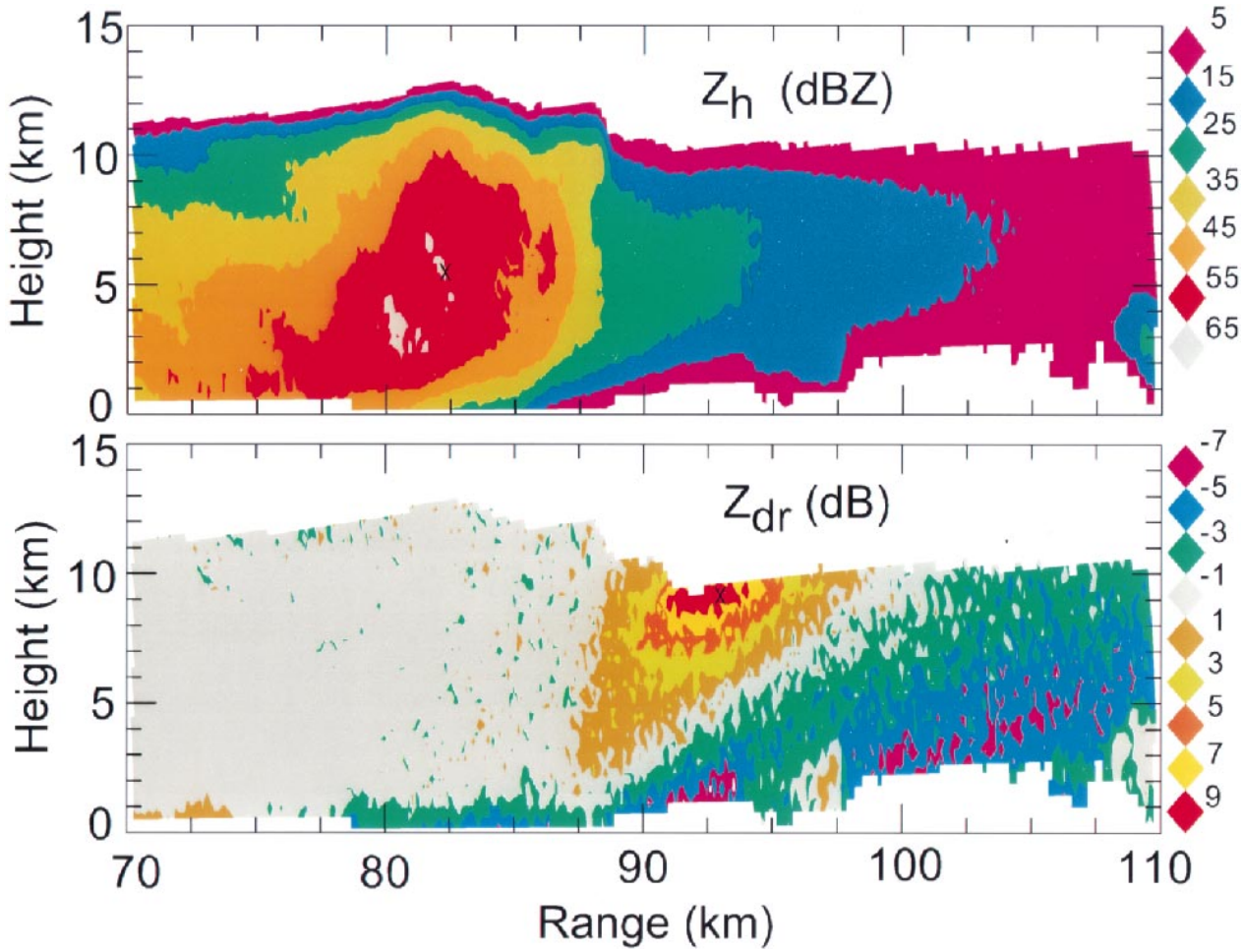

FIG. 1. An example of three-body scattering in a hailstorm from DLR's (German Aerospace Agency) C-band radar located at Oberpfaffenhofen, Germany. The three-body signature is easily seen as the protruding reflectivity area on the right-hand side in the top panel. The bottom panel shows the associated Z_{DR} (differential reflectivity).

Since such negative Z_{DR} signatures are frequently seen in hailshafts, it seems unlikely that they can always be attributed to microphysics. As an alternate explanation, the three-body scatter model calculations described in this paper show that for larger hailstones close to ground level, three-body scattering can bias Z_{DR} negative if ground scatter cross sections are large. The three-body scattering effects are more pronounced at C band than at S band, which agrees with experimental data.

This paper then, explores the effects of three-body scattering on Z_{DR} signatures at S and C bands. Two storm regions are considered: 1) the flare echo region (i.e., the region in back of high-reflectivity cores) and 2) near ground level in hailshafts.

2. Model description

a. General

Zrnić (1987) derived a closed-form solution to predict the reflectivity and velocity signatures of three-body scattering associated with flare echoes. His model included several approximations and simplifications, which are not appropriate for simulating the effects on Z_{DR}. In contrast, we employ a numerical technique, which sums the scattering contributions from all particle pairs that contribute to a particular radar resolution volume, to simulate total power from three-body scatter. The geometry is shown in Fig. 2. The terms P_i and P_j represent two hailstones in the main beam of the radar, while $r_{i,j}$ represent the distance from $P_{i,j}$ to an incremental ground area and $d_{i,j}$ (not shown) represent the distance from $P_{i,j}$ to the radar. The direct scatter comes from the radar resolution volume B_m at a distance R_m from the radar, where R_m terminates at the back edge of the precipitation medium of depth of D. The depth of the resolution volume is controlled by the radar transmit pulse width τ and receiver bandwidth but is given here by $c\tau/2$, where c is the speed of light. Pairs of scatterers in the radar beam will contribute to the observed echo corresponding to B_m if

Unauthenticated | Downloaded 04/13/21 05:55 AM UTC

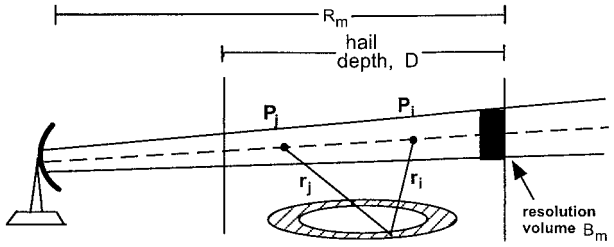

FIG. 2. A schematic of three-body scattering. Signal path: radar → particle P_i → ground → particle P_j → radar. The hatched area represents the area on the ground where the three-body path has the same time delay as the direct path from the radar to the resolution volume B_m.

$$2R_m - c\tau \leq d_i + d_j + r_i + r_j \leq 2R_m. \quad (1)$$

For a given range, R_m and particle pair $P_{i,j}$, the sum $r_i + r_j$ is constant, and thus the loci of particles in 3D space that can contribute to three-body scattering corresponding to range R_m is described by a 3D ellipsoid (prolate spheroid) with the locations of $P_{i,j}$ as the foci.

To simplify the calculations, the following assumptions/simplifications are made: 1) the radar beam is considered to be parallel to ground, 2) the radar beam is modeled as a cylinder with a constant power across the beamwidth, and 3) scatter from a particular incremental volume along the radar beam is approximated by a single scatterer located at the center of the volume along the beam axis. That is, the cylindrical radar beam is subdivided into thin cylinders with a maximum depth of 80 m (a function of radar beam height above the surface). Scatter from this thin cylindrical cross section of the radar beam is modeled by a single scatterer located at the center of the cylinder. Scatter from the hail is modeled by the Mie solution for ice spheres and for water-coated ice spheres.

Under these approximations the above-mentioned ellipsoid will have its $P_{i,j}$ axis parallel to the ground (along the line of sight of the radar) and the intersection of the ellipsoid with the ground will define the ellipse

$$\frac{x^2}{a^2} + \frac{y^2}{b^2} = 1 - \frac{h^2}{b^2}, \quad (2)$$

where $2a$ and $2b$ are the lengths of the major and minor axis of the ellipse, respectively, and h is the distance from the major axis to the ground. The major axis is along the main beam of the radar. The parameters a and b are found from

$$a = \frac{2D - d_i - d_j}{2} \quad \text{and} \quad (3)$$

$$b = [a^2 - (|d_i - d_j|/2)]^{1/2}. \quad (4)$$

The ellipsoid is constrained by the distance from the radar to the back edge of the apparent resolution volume B_m; that is, this distance defines the constant distance $r_i + r_j$ via Eq. (1). Another ellipsoid is defined by the distance from the radar to the front edge of B_m or $R_m - 150$ m for this study. In this way, two concentric, 3D ellipsoids are defined. The intersection of the ground and the concentric ellipsoids is represented by the hatched elliptical shell in Fig. 2. The total power due to three-body scattering corresponding to the B_m resolution volume is found by integrating over all pairs of scatterers that lie in the radar beam and integrating over the corresponding ground areas. Mathematically, for the ith and jth particles,

$$V_{3b} = \frac{g\mathbf{\Omega}^T S_j G_k S_i \mathbf{E}^t}{(4\pi)^2 (R_i R_j r_i r_j)}, \quad (5)$$

where $S_{i,j}$ are 2×2 bistatic scattering matrices for the $P_{i,j}$ particles, G_k is a 2×2 bistatic scattering matrix for a ground element, and g represents an overall system gain constant. Here, $\mathbf{E}^t$ is a 1×2 transmit vector with $[1\ 0]^T$ and $[0\ 1]^T$ representing horizontal and vertical transmit polarization states, while $\mathbf{\Omega}$ is the receive polarization vector of the radar. The scattering matrices for the hail are found from Mie theory and are functions of incident and scattered directions. The total power is found by summing over all particle pairs and over all the corresponding ground areas:

$$P_{3b} = \sum_{i,j} \sum_{k} |V_{3b}|^2. \quad (6)$$

It is important to note that the left summation is a double summation over all particle pairs, which physically means that the three-body scatter path is bidirectional. The direct backscatter power from the resolution volume B_m is calculated for a similar density of scatterers as is used for the three-body scatter calculations:

$$P_{\text{bs}} = \sum_i \frac{g^2 |\mathbf{\Omega}^T S_i \mathbf{E}^t|^2}{(4\pi)^4 d_i^2}. \quad (7)$$

Obviously, summing over a realistic ensemble of hailstones contained in the main beam of a radar would be computationally impossible. To simplify the problem the scatter from a vertical cross section of the radar beam is approximated by a single scatterer located at the center of the volume. Since there is a double summation over particle pairs in Eq. (6) and only a single summation over individual particles in (7), a doubling in the number of particles will increase the power ratio P_{3b}/P_{bs} by 3 dB. The concentration of particles, assumed here to be 1 m^{-3}, is accounted for in the model by increasing the ratio P_{3b}/P_{bs} by the the amount P_{inc}:

$$P_{\text{inc}} = \frac{\text{desired particle number density}}{\text{used particle number density}}. \quad (8)$$

The number density of hail particles as well as the number density of ground grid points was increased until the sum in Eq. (6) converged.

b. Ground model

The most difficult and uncertain part of the analysis is the modeling of the ground, which may be composed

Unauthenticated | Downloaded 04/13/21 05:55 AM UTC

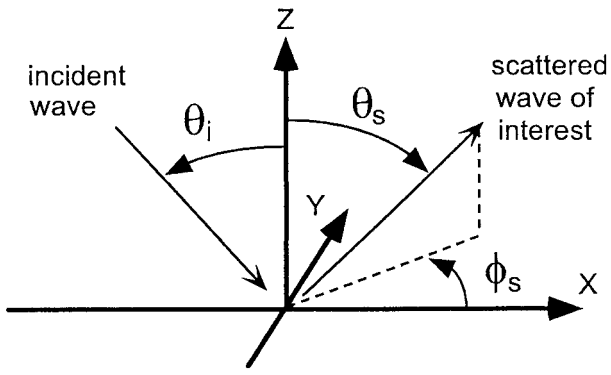

FIG. 3. The three-body scattering geometry for a ground element. Incident wave direction is always in the x–z plane.

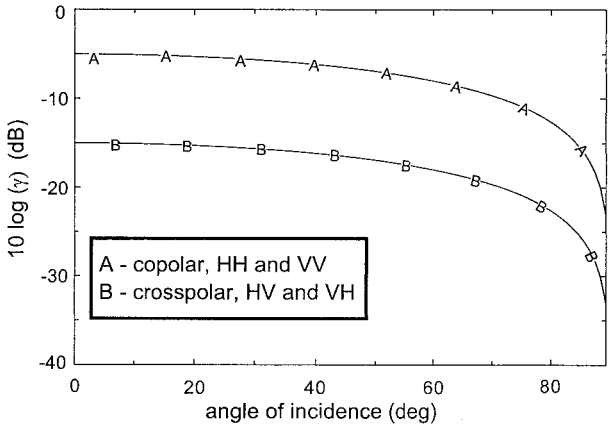

FIG. 4. The backscatter cross section γ for the Lommel–Seeliger model [Eq. (8)] for the ground. Note that $\theta_i = \theta_s$ in Fig. 3.

of trees, shrubs, crops, grasses, roads, buildings, water, etc. Clearly scattering cross sections from such collections vary dramatically. In addition, even though many backscatter measurements have been made at S and C bands, there is a dearth of bistatic measurements. The only significant recent measurements that we are aware of are reported by Ulaby et al. (1988) for 35 GHz. There are sophisticated modeling techniques that have appeared in the literature (Ulaby et al. 1988; Bahar and Zhang 1996), but they would be difficult to implement into our model and would not necessarily yield more accurate or informative solutions due to the general unknown and complex nature of the ground. Therefore, for this general study the computational complexity is reduced by employing two analytical models for rough surfaces: 1) an empirical Lommel–Seeliger model and 2) a statistical model that treats the surface height above a mean planar surface as a random variable. The Lommel–Seeliger model used (Ruck et al. 1970) has the form

$$\gamma(\theta_i, \theta_s) = k \frac{\cos\theta_i + \cos\theta_s}{\cos\theta_i \cos\theta_s}, \tag{9}$$

where k is a function of the surface properties (but treated as a constant here), and θ_i and θ_s are the incident and scattered angles, respectively. Figure 3 shows the bistatic scattering geometry used for the ground models. Vertical (V) incident and scattering directions are defined by the unit vectors $\boldsymbol{\theta}_i$, $\boldsymbol{\theta}_s$, respectively, while horizontal (H) incident and scattering directions are defined by the unit vectors $\boldsymbol{\phi}_i$, $\boldsymbol{\phi}_s$, respectively. The incident vector $\boldsymbol{\theta}_i$ is always in the x–z plane so that $\phi_i = 0$. Note that incident angle defined in a standard spherical coordinate system is typically taken as $\pi - \theta_i$, not θ_i, as is done here (and in Ruck et al. 1970). A plot of the backscatter cross sections (i.e., $\theta_i = \theta_s$, $\phi_s = 180°$) for the Lommel–Seeliger model is shown in Fig. 4. This model gives a reasonable approximation to measured cross sections of terrain surfaces where dimensions are considerably greater than wavelength for diffuse scattering but can be invalid for specular scatter (Ruck et al. 1970). We use it as a first-order approximation in which the copolar H polarization (HH) and copolar V polarization (VV) bistatic cross sections are equal. The advantage of the model is that it is easy to implement, allows for general quantitative results, and lets Z_{DR} calculation be unbiased from ground effects (i.e., VV = HH and VH = HV for ground scatter cross sections).

The statistical model is actually an algebraic combination of two models for rough surfaces: 1) a model valid for slightly rough surfaces; and 2) a model valid for very rough surfaces where slightly rough means that the rms surface height is much less than the wavelength, while very rough means that the rms surface height is much greater than the wavelength. Typical terrain surfaces will be composed of roughnesses of both scales for frequencies considered here and thus the models are combined with the resulting model yielding scattering cross sections that give good approximation to experimental data (Ulaby and Dobson 1989). Importantly, the VV exceeds the HH backscatter cross section, which is frequently observed experimentally and is necessary here to obtain significant negative Z_{DR} in hailshafts at near–ground levels. The statistical model, while giving a more accurate representation of terrain than the above Lommel–Seeliger model, is still analytical, which thus allows for fairly simple simulations. Details of the statistical model can be found in the appendix.

Shown in Fig. 5a are backscatter cross sections for the slightly rough surface and the very rough surface models. The slightly rough surface model has the VV cross section greater than the HH cross section for angles greater than about 10°. The very rough surface model has the VV and HH backscatter cross sections equal and has larger cross sections for angles less than 10°. The composite model shown in Fig. 5b is found by simply adding the backscatter amplitudes from the two models. Experimental measurements reported in Ulaby and Dobson (1989) indicate that the composite curves shown in Fig. 5b are quite realistic and, furthermore, the curves could be easily increased several decibels in magnitude especially at small incidence an-

Unauthenticated | Downloaded 04/13/21 05:55 AM UTC

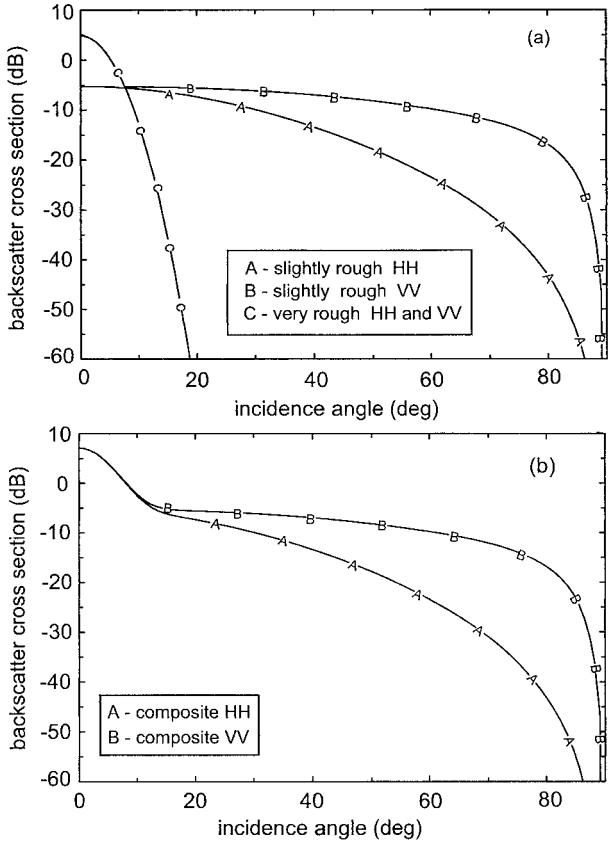

FIG. 5. The backscatter cross section ($\theta_i = \theta_s$) for (a) the very rough and slightly rough surface models and (b) the composite model.

gles. The parameters chosen for the composite model are $k_0 l = 1.5$, $k_0 h = 0.3$, and $w = 0.087\,49$. The dielectric constant used for the ground is $e_r = 48.82 + j15.12$ for both S and C band, which was calculated from a formula given in Ruck et al. [1970, their Eqs. (9.1)–(41)] The parameters were chosen based more on the final shape of the resulting composite curve rather than on some physical criterion. The most important result is that the theoretical model used here approximates known experimental measurements.

3. Simulation results

a. Z_{DR} signatures on the back side of a hailshaft

The two primary factors affecting the nature of three-body Z_{DR} signatures are 1) the difference in the scattering characteristics of hail at V and H incident polarizations and 2) the scattering characteristics of the ground. We first illustrate how scattering characteristics of hail affect Z_{DR} on the back side of high reflectivity cores by examining the field patterns of horizontally and vertically oriented dipoles, which are used as simple models for the scattered fields of hailstones. Figure 6 shows a dipole scatterer located above the *x–y* plane

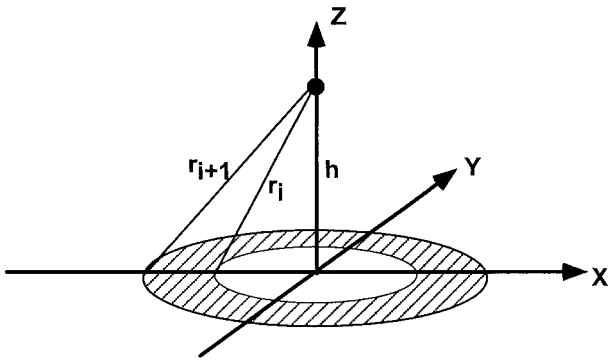

FIG. 6. Geometry for dipole field calculation. Dipole is located at height h above *x–y* plane. Incident wave is along the positive x direction. The lengths r_i, r_{i+1} define an area between concentric circles over which power from the vertical and horizontal dipole fields are summed.

(the ground) coincident with z axis with $z = h$, where h here refers to the height above the *x–y* plane. Concentric circles are shown on the *x–y* plane defined by varying the length of r by 0.15 increments (arbitrary units). The incident wave is in the positive x direction along the line defined by $z = h$, $y = 0$. The 3D plot of the scattered field intensity for incident V polarization resembles a horizontal ''doughnut'' (e.g., see 3D dipole field pattern in Balanis 1982) with maximum intensity loci in the horizontal plane defined by $z = h$ and minimum intensity (zero) along the z axis. For H-incident polarization the maximum intensity is located in the *x–z* plane and the minimum intensity is along the line defined by $x = 0$, $z = h$. Thus a horizontal dipole will have an intensity maximum in the negative z direction, while a vertical dipole will have a minimum (zero). Figure 7 shows the ratio of H to V total dipole power incident on the area defined by the concentric circles $r_i = 0.15i$ and $r_{i+1} = 0.15(i + 1)$, $(i = 1, 2, 3, \ldots)$ with the dipole height h as a parameter. The horizontal axis is r_i. As the diameter of the concentric circles becomes

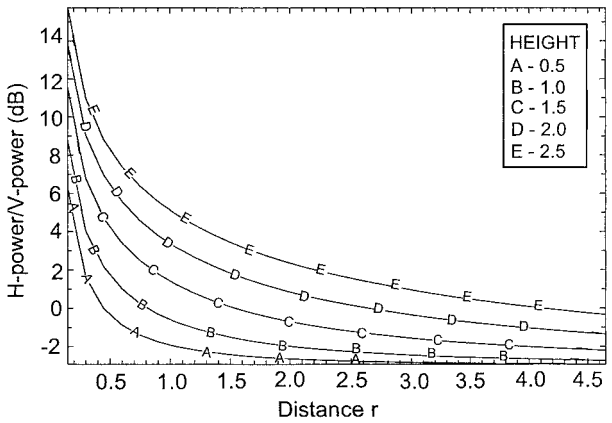

FIG. 7. The ratio of horizontal to vertical power incident on the hatched area in Fig. 6 with h as a parameter. The horizontal axis is in arbitrary units of r_i and $r_{i+1} = 0.15 + r_i$.

Unauthenticated | Downloaded 04/13/21 05:55 AM UTC

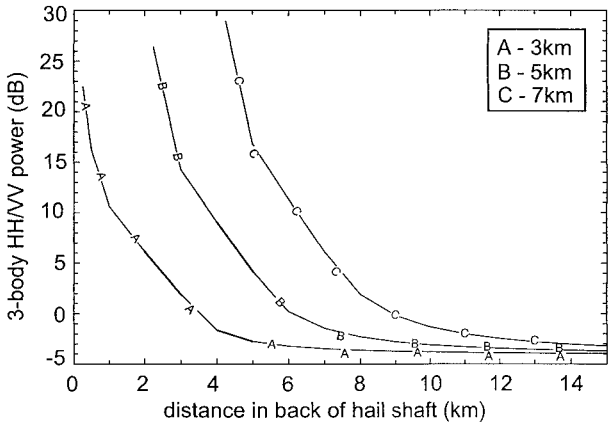

FIG. 8. The three-body power ratio HH/VV as a function of distance in back of the hailshaft.

larger, the ratio of H to V power becomes smaller. This suggests (to the extent that a dipole field resembles scatter from hail) that three-body Z_{DR} in back of a hailshaft will have a tendency to go from positive to negative as range increases. This type of Z_{DR} pattern is observed in Fig. 1 at ranges 88–110 km at heights of 3–10 km.

The full three-body scattering model described in section 2, which uses the Lommel–Seeliger ground model, is now used to calculate the three-body Z_{DR} signatures on the back side of a hailshaft. The hailshaft depth, D_p, is 3 km and the hail is modeled as 2-cm solid ice spheres. Shown in Fig. 8 is the ratio of three-body HH power to three-body VV power as a function of range from the back (away from the radar) of the hailshaft (i.e., 0 km corresponds to the back edge of the hailshaft). The three curves correspond to 3-, 5-, and 7-km radar beam heights above ground. The curves show that the three-body Z_{DR} values are very high close to the hailshaft and then decrease monotonically with increasing range and become negative. As the height increases, the range at which the Z_{DR} first becomes negative increases. This is similar to what is observed in Fig. 1. Thus, the three-body Z_{DR} signature on the back of hailshafts can be attributed to the angular scattering pattern of the hailstones with no preferential scattering from the ground (i.e., VV $>$ HH ground cross sections) required.

b. Negative Z_{DR} in hailshafts

The model is now used to investigate Z_{DR} signatures in hailshafts at low elevations. A two-layer model is used for the spherical hail: a solid spherical ice core is covered with a 1-mm liquid water shell, which is a typical way to model melting hail (Rassumssen and Heymsfield 1987). The ground is first described using the Lommel–Seeliger model given by Eq. (9). There are two conditions to be met if three-body scattering is to bias the observed Z_{DR} to negative values: 1) the power due to three-body scattering must be close in magnitude to the power due to direct backscatter; and 2) the VV three-body power must be greater than the HH three-body power in order to cause negative observed Z_{DR} (Z_{DR}^{obs}), with

$$Z_{DR}^{obs} = 10 \log\left[\frac{P_{hh}^{bs} + P_{hh}^{3b}}{P_{vv}^{bs} + P_{vv}^{3b}}\right], \tag{10}$$

where P_{hh}^{bs} and P_{vv}^{bs} are the direct backscattered copolar powers at H- and V-incident polarizations (equal for spherical scatterers), and P_{hh}^{3b} and P_{vv}^{3b} are the three-body copolar powers for H- and V-incident polarizations, respectively. Suppose that $P_{vv}^{bs} = P_{hh}^{bs} = P_{vv}^{3b} = 2P_{hh}^{3b}$; for example, the direct backscatter medium consists of randomly oriented hail (intrinsic $Z_{DR} = 0$ dB) with the VV three-body power exceeding the HH three-body power by 3 dB. In this case the $Z_{DR}^{obs} = -1.25$ dB. If the three-body Z_{DR} is made 3 dB more negative, that is, $P_{vv}^{3b} = 4P_{hh}^{3b}$ instead of $P_{vv}^{3b} = 2P_{hh}^{3b}$, then the three-body VV power can also be 3 dB less, that is, $P_{vv}^{bs} = P_{hh}^{bs} = 2P_{vv}^{3b}$, and these values still yield $Z_{DR}^{obs} = -1.25$ dB. Thus, the three-body VV power can be 3 dB less than the direct backscatter power and still significantly bias the observed Z_{DR}.

Figure 9 shows modeling results using the Lommel–Seeliger ground model for panel (a) S band and panel (b) C band. There are three sets of curves in each plot corresponding to radar beam heights at 0.01-, 0.1-, and 0.5-km heights above ground. Obviously, if the center of the radar beam is at 0.01 or 0.1 km, the lower part of the beam would be blocked by the earth (assuming a 1° beamwidth). The model assumes no beam blockage and is meant to demonstrate the effects of low elevation angles. The horizontal axis is the diameter of the hail, while the left vertical axis (solid curves) shows the ratio of VV three-body power to VV direct backscatter power (in dB), and the right vertical axis (dashed curves) is three-body Z_{DR} (P_{hh}^{3b}/P_{vv}^{3b}) (in dB). The dashed curves are not distinguished since they are similar and show that three-body Z_{DR} is typically close to zero ($|Z_{DR}| < 0.7$ dB) for this model. For S band $P_{vv}^{3b} > P_{vv}^{bs}$ for $D > 4$ cm at 0.01-km height. At 0.5-km height $P_{vv}^{3b} > P_{vv}^{bs}$ only for $d = 5.5$ cm. The model indicates that hail with diameters of about 5–6 cm would most likely provide sufficient power in order for the three-body scatter to be large enough to effect the primary backscatter signal. Hail less than about 3.5 cm is much less likely to cause enough three-body power to affect the primary backscatter return. At C band, however, there is a peak at $D = 2.75$ cm, where $P_{vv}^{3b} > P_{vv}^{bs}$ at 0.01-, 0.1-, and 0.5-km heights with $P_{vv}^{3b}/P_{vv}^{bs} = 22.9$ dB for $h = 0.01$ km. Figure 9 also suggests that three-body scattering effects will be more evident at C band than at S band since the occurrence of 2.5–3-cm hail is much more common than 5–6-cm hail. Since three-body Z_{DR} (dotted curves) are not negative enough to significantly bias Z_{DR}^{obs}, we next use the statistical ground model in order to obtain negative Z_{DR}^{obs}.

Figure 10 is similar to Fig. 9 but with the statistical

Unauthenticated | Downloaded 04/13/21 05:55 AM UTC

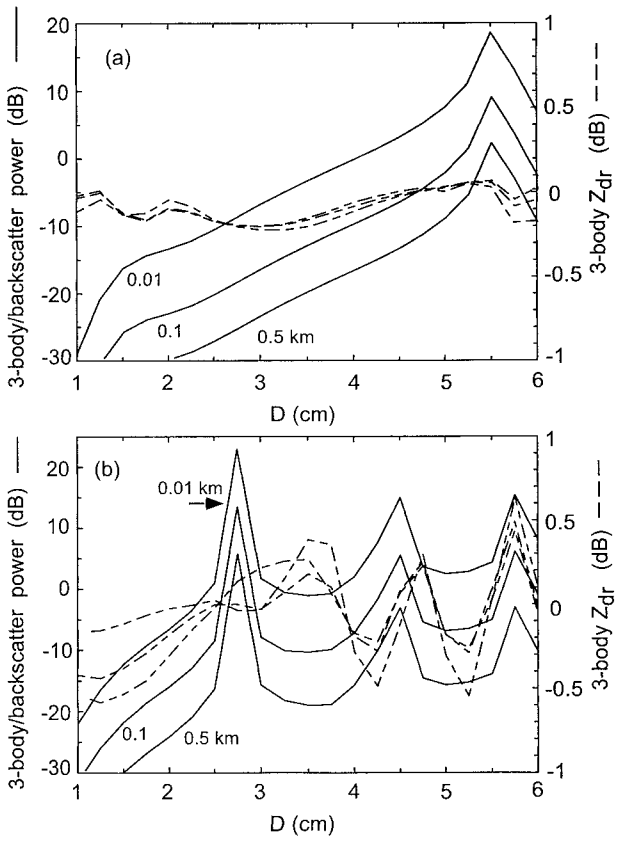

FIG. 9. The ratio of three-body scatter power to direct backscatter power (left axis) and three-body Z_{DR} as a function of hail diameter. Spherical hail is modeled as an ice core with a liquid water coat (1 mm). The Lommel–Seeliger ground model is used at (a) S band and (b) C band.

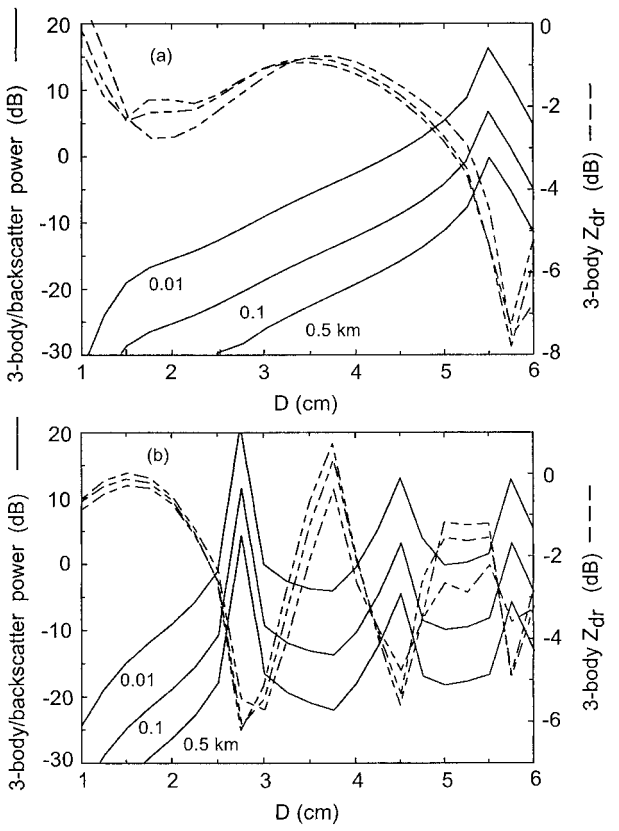

FIG. 10. As in Fig. 9, except the statistical ground model is used.

ground model used in place of the Lommel–Seeliger ground model. The solid curves are similar in shape and magnitude to the solid curves of Fig. 9 and similar conclusions can be drawn. However, the dotted curves, showing three-body Z_{DR}, are now quite negative especially in the resonant regions of interest, that is, $D >$ 4 cm for S band and 2.5 cm $< D <$ 3 cm for C band. Thus, the more realistic statistical ground model provides for negative three-body Z_{DR} that can cause Z_{DR}^{obs} to be negative. Again, VV are frequently greater than HH ground cross sections for many different terrain types (Ulaby and Dobson 1989).

Use of the water-coated ice model for melting hail is not necessary to obtain $P_{vv}^{3b}/P_{vv}^{bs} > 1.0$. To illustrate this, the hail is modeled as ''spongy ice'' using various ice/water ratios (Bohren and Batten 1982) at S band. Shown in Fig. 11 is the ratio of three-body power to direct backscatter power for hail modeled as 80% ice, 20% water; 90% ice, 10% water; 95%, ice 5% water; solid ice; and the two-layer (water-coated) model used in Fig. 10. All curves exhibit peaks above 0 dB for $D > 4$ cm except the curve for 95% ice, 5% water. Thus a variety of dielectric constants for hail will produce $P_{vv}^{3b} > P_{vv}^{bs}$.

4. Model modifications

a. Three-body power as a function of height

As shown in Figs. 9 and 10 the ratio of three-body power to direct backscatter power ($P_R = P_{vv}^{3b}/P_{vv}^{bs}$) is a strong function of height and will vary significantly across the vertical dimension of the radar beam. To ac-

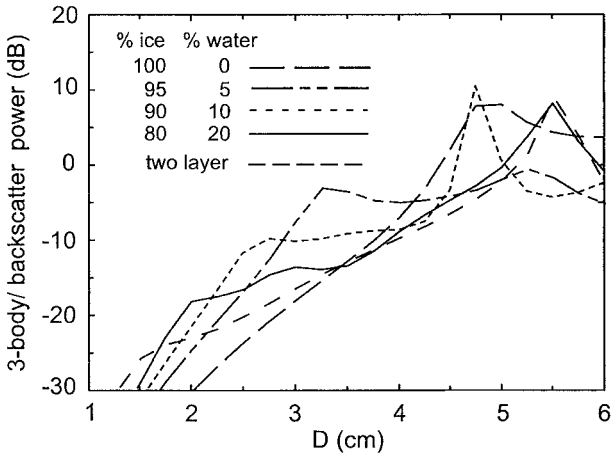

FIG. 11. The ratio of three-body scatter power to direct backscatter power for various mixtures of ice and water. Two-layer denotes water-coated ice spheres.

Unauthenticated | Downloaded 04/13/21 05:55 AM UTC

count for this the P_R is integrated numerically across the beamwidth as a function of height. The cylindrical radar beam is divided into eight sections of equal height with P_R at the center of the sections found by interpolation from the previous calculated P_R at heights of 0.01, 0.01, and 0.5 km. These power ratios (in linear scale) are, approximately, proportional to h^{-1}. The radar beam is taken to be 0.5 km in diameter (i.e., a 1° beamwidth at about 30-km range) and is centered at 0.25 km above ground (e.g., a 0.5° elevation angle). The integration at S band for $D = 5.5$ cm and at C band for $D = 2.75$ cm and for the statistical ground model gives P_R as 5 and 9.5 dB, respectively. In comparison, using the previous model that places hail only at the center of the beam (at 0.25-km height) gives P_R as 2.5 and 7.3 dB, respectively. If the center of the beam is at 0.5-km height (≈1° elevation angle), the beamwidth-integrated P_R become −0.2 and 4.6 dB, respectively, as compared to −0.5 and 4.2 dB, respectively, if the hail is located only at the center of the radar beam. Thus, the integration across the beam of the radar only changes the power ratio by no more that 2.5 dB for these two cases but does increase the P_R in all cases. Note that because P_R is proportional to h^{-1}, the closer the center of the radar beam is to the ground, the more likely the three-body power will affect the observed radar signals.

b. Hail size distribution

To study the effect of integration over a size distribution, the three-body power from a distribution consisting of just two sizes with equal number of particles in each class is considered first. The three-body power is expressed as

$$P_{3b} = \sum_{i,j}\sum_{k} \alpha_i G_k \alpha_j + \sum_{i,j}\sum_{k} \beta_i G_k \beta_j + 2\sum_{i,j}\sum_{k} \alpha_i G_k \beta_j, \quad (11)$$

where α and β are the scattering amplitudes for the two size classes. The computation time required for a distribution of particles sizes would be unfeasible (unless the number of particles sizes is kept very small), and therefore an estimation of the power from the interaction of the two classes is used. The first two summations are known from previous monodisperse calculations and the third summation, which accounts for the interaction between the two classes, is estimated from

$$\sum_{i,j}\sum_{k} \alpha_i G_k \beta_j = \left(\left\{\sum_{i,j}\sum_{k} \alpha_i G_k \alpha_j\right\}\left\{\sum_{i,j}\sum_{k} \beta_i G_k \beta_j\right\}\right)^{1/2}. \quad (12)$$

This approximation assumes that three-body power from the monodisperse distributions bound the sum representing the three-body power from the interaction of the two classes and can be estimated by Eq. (12), which is the geometric mean of the three-body powers for the two monodisperse distributions. Using Eq. (12) along with Eq. (11), the total three-body power can be estimated. The total direct backscatter power is found from the simple (incoherent) addition of the backscatter powers of the individual size classes. This estimation method increases the particle density by a factor of 2 (for a size distribution with two distinct classes) and this is accounted for by an adjustment of the particle density factor by 0.5 for this case. It is a simple matter to expand this method to an arbitrary number of hail sizes. In this way the number density of the total population of particles is kept at 1 m^{-3} with each size class having equal number densities. For S band, particle sizes from 4 to 5.5 cm are integrated for hail modeled as water-coated ice spheres. Using the statistical ground model, a beamwidth of 0.5-km diameter, a beam height 0.25 km, and powers derived above by integrating across the radar beam, the resulting power ratio is $P_R = -9.4$ dB. A similar integration at C band but for particles sizes of 2.5, 2.75, and 3.0 cm yields $P_R = -11.8$ dB. This low value may be unexpected since P_R is quite high (about 11 dB for $h = 0.1$ km; see Fig. 10b) for $D = 2.75$ cm at C band. This large value, 11 dB, is more a result of the reduction of direct backscatter power than a large increase in three-body power. For these particular size distributions, the power ratios P_R need to be increased about 6–8 dB to bring them to the −3-dB level, where three-body scattering can significantly effect observed Z_{DR}. The needed additional power could be obtained by increasing the scattering cross sections of the ground. Ulaby and Dobson (1989) show backscatter cross sections for grasses at S band, which have the 95% occurrence level curve at about 16 dB for vertical incidence backscatter with the similar curve for C band at 13 dB. In other words, 5% of the experimental observations exceeded these levels. In comparison, the statistical ground model parameters assumed here gave backscatter cross sections of about 5 dB at vertical incidence. Furthermore, the Ulaby and Dobson VV curves typically lie above the HH curves especially at small incident angles and more so at C band than at S band. The statistical model parameters used here gave equal VV and HH cross sections for small (<10°) incidence angles (see Fig. 5). Additional three-body power can be gained by increasing the size of the radar resolution volume. The modeled uses a radar resolution volume based on a 1° beamwidth at 30-km range. If the range is doubled, the size of resolution volume is increased by a factor of 4, and this increase in volume (assuming the hail density remains at 1 m^{-3}) will increase P_R by 6 dB due to the double summation (over particle pairs) in Eq. (6). Thus 6 dB of additional power is gained by simply increasing the range of the hailshaft to 60 km; however, similarly P_R is reduced by 6 dB by decreasing the range to the hailshaft to 15 km. In any event, it is quite possible that conditions for strong three-body scattering do occur according to the models used and the experimental observations. This, however, does not preclude other factors that can cause negative Z_{DR} via direct backscatter due to shape and orientation effects. Negative Z_{DR} could also be caused by

Unauthenticated | Downloaded 04/13/21 05:55 AM UTC

differential attenuation (A_{DP}) due to by rain along the propagation path, high reflectivity gradients across the antenna beam and sidelobes, direct backscatter from the ground, or a combination of these factors. In fact, A_{DP} and three-body scattering can produce similar Z_{DR} signatures on the back side of high-reflectivity areas at low-elevation angles. The A_{DP} lowers the observed Z_{DR} according to $Z_{DR}^{obs} = Z_{DR} - (2A_{DP})r$, where Z_{DR} represents the intrinsic Z_{DR} of the medium r is the range (in km) and A_{DP} is the one-way differential attenuation (in dB km^{-1}) for an aligned medium. To distinguish between these two mechanisms, the LDR (linear depolarization ratio) as a function of range can be examined if available. If the LDR_h (LDR_h is VH/HH, while LDR_v is HV/VV) is very high, say, greater than -15 dB, and the reflectivity is low ($Z < 35$ dBZ), three-body scattering is very likely causing the negative Z_{DR} since intrinsic scatterers that would cause the low reflectivity would likely have much lower LDR (e.g., light rain, ice crystals, dry graupel). Also, the A_{DP} can be estimated from the copolar specific differential phase (K_{DP}), which is the slope of the range profile of copolar differential phase (ϕ_{DP}) (Bringi et al. 1990) by $A_{DP} = \beta K_{DP}$ with $\beta = 0.003\,67$ at S band and $\beta = 0.0157$ at C band. However, recent experimental evidence (Ryzhkov and Zrnić 1995; Carey et al. 1997) suggests that the results in Bringi et al. (1990) may underestimate, in some cases, the amount of differential attenuation per degree of differential phase by a factor of 2. For the C-band case shown in Fig. 1, the total ϕ_{DP} through the main precipitation shaft was about 40°, so that the amount of differential attenuation could be 1.26 dB if β in the relationship, as given by Bringi et al. (1990), is doubled. This still cannot account for the -2 dB and smaller Z_{DR} values observed close to ground level. In addition, LDR is high, ranging from about -16 to -6 dB, and the ρ_{hv} (copolar correlation coefficient) is quite low, ranging from about 0.1 to 0.4 in this area, which also suggests three-body scatter. In areas where three-body scattering clearly dominates (e.g., in the flare echo regions) LDR is typically -5 dB or higher and ρ_{hv} is low, that is, less than 0.8 and more typically 0.5 or less. These signatures are due to the scattering characteristics of the ground. If the negative Z_{DR} was due to vertically aligned oblate or prolate hail, then such low LDR and ρ_{hv} would be unlikely. In addition, differential attenuation will cause LDR_h to increase, while LDR_v will *decrease* and thus this can be another check for the presence of differential attenuation.

5. Conclusions

The three-body reflectivity signatures known as flare echoes or ''hail spikes'' are routinely seen on the back side of high-reflectivity cores that contain hail. However, the effects of three-body scattering on differential reflectivity (Z_{DR}) are not as well known. It is important to understand the possible origin of these signatures, especially for future operational systems (e.g., Zahrai and Zrnić 1997). This paper used a numerical model to investigate the effects of three-body scatter on Z_{DR} signatures. Scattering from spherical hailstones was modeled using Mie theory, while a general Lommel–Seeliger and a statistical model were used to represent scattering from the ground. The Lommel–Seeliger model shows VV and HH cross sections to be equal (as well as VH and HV). This model was sufficient to explain the Z_{DR} signature seen on the back side of the hail core shown in Fig. 1. This model was also used to investigate the possible effects of three-body scatter at low-elevation angles within hail cores. At very low elevations large hail produced enough three-body power to affect the primary backscatter signal. However, the model also showed that three-body Z_{DR} was about 0 dB so that the intrinsic Z_{DR} would not be significantly biased negative (or positive). A more accurate statistical-based ground model was then employed that provided for VV ground cross sections to exceed HH ground cross sections, which is frequently observed experimentally (Ulaby and Dobson 1989). Using this ground model caused three-body Z_{DR} to be quite negative, and thus three-body scattering was shown to be a possible explanation for the frequently observed negative Z_{DR} close to ground in hailshafts. The hail size that gave the greatest three-body scatter power to direct backscatter power ratio (P_R) was around 2.75 cm for C band and 5.5 cm at S band for hail modeled as water-coated ice spheres. Hail was also modeled as ice spheres with various dielectric constants, and the results showed that such hailstones also yielded P_R values similar to values for water-coated ice so that a wide variety of hailstone types will yield similar three-body powers. The effects of three-body scattering at low elevations would most likely be observed on the back edge of hailshafts where the three-body scattering would remain strong but where the direct scatter from hail has decreased due to decreased concentration of hail. Also, due to the bidirectional nature of three-body scatter, the larger the radar resolution volume, the larger the power ratio P_R becomes since backscatter power increases by n (number of hydrometeors), while three-body power increases by n^2. This means that three-body signatures become stronger with increased range, all other factors being equal. It is also possible that if HH ground cross sections were to exceed VV ground cross sections, Z_{DR} would be biased positive.

To distinguish negative Z_{DR} caused by three-body scattering from negative Z_{DR} caused by differential attenuation (A_{DP}) due to rain, especially on the back side of storm cores, the differential phase (ϕ_{DP}), linear depolarization ratio (LDR), and copolar correlation coefficient (ρ_{hv}) signatures can be examined. The amount of A_{DP} due to rain can be estimated from the ϕ_{DP} so that the amount of negative Z_{DR} due to A_{DP} can be also estimated. Recent studies (Ryzhkov and Zrnić 1995; Carey et al. 1997) have shown that more A_{DP} can occur (about a factor of 2) than what is predicted from ϕ_{DP} according to relationships given in Bringi et al. (1990). If the observed Z_{DR} is more negative than that predicted

Unauthenticated | Downloaded 04/13/21 05:55 AM UTC

by A_{DP}, then other possible causes need to be considered, including three-body scatter. In flare echo regions where three-body scattering clearly dominates, the observed LDR was extremely high, −10 to 0 dB, and ρ_{hv} was very low at less than 0.8 and typically around 0.5 or less. Thus, if the LDR is higher and the ρ_{hv} lower than can be explained by the type of hydrometeors present, then three-body scatter could be an alternate explanation. In contrast, differential attenuation does not effect ρ_{hv} and only increases LDR by $A_{DP}r$, where r is the range along the rain filled propagation path (assuming that the propagation matrix is diagonal). Unfortunately, LDR can be high (and ρ_{hv} can be low) due to direct backscatter from hail but typically not as high (or low) as that seen for three-body scattering. Note that other factors, such as steep reflectivity gradients (along with mismatched copolar antenna patterns; e.g., see Hubbert et al. 1998) and clutter, can also have similar effects. The end result is that it can be very difficult to identify and especially separate these various effects.

Acknowledgments. The authors acknowledge support from the National Science Foundation and the U.S. Weather Research Program via ATM-9612519. The DLR C-band radar data were made available through Dr. Peter Meischner.

APPENDIX

Statistical Rough Surface Model

The two statistical rough surface models are given. They are combined to make the composite rough surface model used in the study.

a. Slightly rough surface model

The solution given here for a slightly rough surface was formulated by Rice (1965) and derived by Peake (1959a,b) employing a perturbation technique and can be found in Ruck et al. (1970). It is important to note that the present application is valid for polarization-dependent bistatic scatter.

The average (incoherent) scattering amplitude per unit surface area is

$$s_{pq} = \frac{4}{\pi} k_0^2 h \cos\theta_i \cos\theta_s \alpha_{pq} I, \tag{A1}$$

where p, q represent the scattered and incident polarization states, respectively; h is the square root of the mean-square roughness height; k_0 is the wavenumber; α_{pq} (given below) is directly proportional to the scattering matrix element. The quantity I is given here for a Gaussian surface-height correlation coefficient (Ruck et al. 1970):

$$I = \pi l \exp\left[\frac{-k_0^2 l^2 (\xi_x^2 + \xi_y^2)}{2}\right], \tag{A2}$$

where

$$\xi_x = \sin\theta_i - \sin\theta_s \cos\phi_s, \tag{A3}$$

$$\xi_y = \sin\theta_i \sin\theta_s, \tag{A4}$$

and the quantity l is the correlation length. The bistatic scattering elements, α_{pq}, for H and V polarizations are

$$\alpha_{hh} = -\frac{(\epsilon_r - 1)\cos\phi_s}{(\cos\theta_i + \sqrt{\epsilon_r - \sin^2\theta_i})(\cos\theta_s + \sqrt{\epsilon_r - \sin^2\theta_s})}, \tag{A5}$$

$$\alpha_{vh} = -\frac{\sin\phi_s(\epsilon_r - 1)\sqrt{\epsilon_r - \sin^2\theta_s}}{(\cos\theta_i + \sqrt{\epsilon_r - \sin^2\theta_i})(\epsilon_r \cos\theta_s + \sqrt{\epsilon_r - \sin^2\theta_s})}, \tag{A6}$$

$$\alpha_{hv} = \frac{\sin\phi_s(\epsilon_r - 1)\sqrt{\epsilon_r - \sin^2\theta_i}}{(\epsilon_r \cos\theta_i + \sqrt{\epsilon_r - \sin^2\theta_i})(\cos\theta_s + \sqrt{\epsilon_r - \sin^2\theta_s})}, \quad \text{and} \tag{A7}$$

$$\alpha_{vv} = \frac{(\epsilon_r - 1)[\epsilon_r \sin\theta_s \sin\theta_s - \cos\phi_s\sqrt{\epsilon_r - \sin^2\theta_i}\sqrt{\epsilon_r - \sin^2\theta_s}]}{(\epsilon_r \cos\theta_i + \sqrt{\epsilon_r - \sin^2\theta_i})(\epsilon_r \cos\theta_s + \sqrt{\epsilon_r - \sin^2\theta_s})}. \tag{A8}$$

The dielectric constant, ϵ_τ used for both S and C bands is $48.8152 + 15.12i$, which was calculated from (Peake 1959a; Ruck et al. 1970)

$$\epsilon_\tau = 2.5(1 - f) + f\epsilon_{\tau w}, \tag{A9}$$

where $\epsilon_{\tau w}$ is the dielectric constant for water taken here as $77.90 + i13.24$ and f is the fraction of water by weight present in the vegetation, which is taken as 60% here. Since hail will typically be falling on ground that is wet from accompanying rain, this is reasonable assumption even if the vegetation was previously dry. Wetting of the ground will, in general, increase the magnitude of the cross sections of the ground (Ulaby and Dobson 1989).

Unauthenticated | Downloaded 04/13/21 05:55 AM UTC

b. Very rough surface model

As the surface roughness increases with respect to wavelength, the scattered field becomes more incoherent. A specular-point model is employed in which it is assumed that scattered field results from areas that specularly reflect the incident wave. This is also referred to as an optic approach (Ruck et al. 1970). The bistatic scattering amplitudes are

$$S_{pq} = \beta_{pq} J, \tag{A10}$$

where p, q refer to polarization states, β is proportional to the scattering matrix element, and J is defined as

$$J = \frac{2}{w\xi} \exp\left[-\frac{\xi_x^2 + \xi_y^2}{2w\xi_z^2}\right], \tag{A11}$$

where $w^2 = 4h^2/l^2$, h^2 is the mean-square roughness height and l is the surface correlation length. The terms $\xi_{x,y}$ are defined in Eqs. (A3) and (A4), respectively, and

$$\xi_z = -\cos\theta_i - \cos\theta_s. \tag{A12}$$

The scattering matrix elements for the H–V basis are

$$\beta_{vv} = \frac{a_2 a_3 R_\parallel(\iota) + \sin\theta_i \sin\theta_s \sin^2\phi_s R_\perp(\iota)}{a_1 a_4} \tag{A13}$$

$$\beta_{hv} = \sin\phi_s \frac{-\sin\theta_i a_3 R_\parallel(\iota) + \sin\theta_s a_2 R_\perp(\iota)}{a_1 a_4} \tag{A14}$$

$$\beta_{vh} = \sin\phi_s \frac{\sin\theta_s a_2 R_\parallel(\iota) - \sin\theta_i a_3 R_\perp(\iota)}{a_1 a_4} \tag{A15}$$

$$\beta_{hh} = \frac{-\sin\theta_i \sin\theta_s \sin\phi_s R_\parallel(\iota) - a_2 a_3 R_\perp(\iota)}{a_1 a_4}, \tag{A16}$$

where $R_\perp(\iota)$, $R_\parallel(\iota)$ are Fresnel reflection coefficients

$$R_\parallel(\iota) = \frac{\epsilon_r \cos\iota - \sqrt{\epsilon_r - \sin^2\iota}}{\epsilon_r \cos\iota + \sqrt{\epsilon_r - \sin^2\iota}} \tag{A17}$$

$$R_\perp(\iota) = \frac{\cos\iota - \sqrt{\epsilon_r - \sin^2\iota}}{\cos\iota + \sqrt{\epsilon_r - \sin^2\iota}}, \tag{A18}$$

with ϵ_τ being the relative permittivity (the relative permeability has been assumed to be unity). The angles of incidence argument ι for the Fresnel coefficients and the other quantities are defined as

$$\cos\iota = \frac{1}{\sqrt{2}}\sqrt{1 - \sin\theta_i \sin\theta_s \cos\phi_s + \cos\theta_i \cos\theta_s} \tag{A19}$$

$$a_1 = 1 + \sin\theta_i \sin\theta_s \cos\phi_s - \cos\theta_i \cos\theta_s \tag{A20}$$

$$a_2 = \cos\theta_i \sin\theta_s + \sin\theta_i \cos\theta_s \cos\phi_s \tag{A21}$$

$$a_3 = \sin\theta_i \cos\theta_s + \cos\theta_i \sin\theta_s \cos\phi_s \tag{A22}$$

$$a_4 = \cos\theta_i + \cos\theta_s. \tag{A23}$$

The composite rough surface model is a simple addition of the above two models.

REFERENCES

Aydin, K., and Y. Zhao, 1990: A computational study of polarimetric radar observables in hail. *IEEE Trans. Geosci. Remote Sens.*, **28,** 412–421.

——, A. Seliga, and V. N. Bringi, 1984: Differential radar scattering properties of model hail and mixed phase hydrometeors. *Radio Sci.*, **19,** 58–66.

Bahar, E., and Y. Zhang, 1996: A new unified full wave approach to evaluate the scatter cross sections of composite rough surfaces. *IEEE Trans. Geosci. Remote Sens.*, **34,** 973–980.

Balanis, C. A., 1982: *Antenna Theory: Analysis and Design.* Harper and Row, 790 pp.

Bohren, C. F., and L. J. Batten, 1982: Radar backscattering of microwaves by spongy ice spheres. *J. Atmos. Sci.,* **39,** 2623–2628.

Bringi, V. N., T. A. Seliga, and K. Aydin, 1984: Hail detection using a differential reflectivity radar. *Science,* **225,** 1145–1147.

——, V. Chandrasekar, N. Balakrishnan, and D. S. Zrnić, 1990: An examination of propagation effects in rainfall on radar measurements at microwave frequencies. *J. Atmos. Oceanic Technol.,* **7,** 829–840.

Carey, L. D., S. A. Rutledge, and T. D. Keenan, 1997: Correction of attenuation and differential attenuation at S- and C-band using differential propagation phase. Preprints, *28th Int. Conf. on Radar Meteorology,* Austin, TX., Amer. Meteor. Soc., 25–26.

Hubbert, J., V. N. Bringi, L. D. Carey, and S. Bolen, 1998: CSU–CHILL polarimetric radar measurements in a severe hailstorm in eastern Colorado. *J. Appl. Meteor.*, **37,** 749–775.

Peake, W. H., 1959a: The interaction of electromagnetic waves with some natural surfaces. Tech. Rep. 898-2, Antenna Laboratory, Ohio State University, 110 pp. [Available from Electroscience Laboratory, Ohio State University, 1320 Kinnear Rd., Columbus, OH 43212.]

——, 1959b: Theory of radar return from terrain. IRE National Convention Record 7, Part 1, 27–41.

Rasmussen, R. M., and A. J. Heymsfield, 1987: Melting and shedding of graupel and hail. Part I: Model physics. *J. Atmos. Sci.*, **44,** 2754–2763.

Rice, S. O., 1965: Reflection of electromagnectic waves by a slightly rough surface. *The Theory of Electromagnetic Waves,* M. Kline, Ed., Dover, 351–378.

Ruck, G., D. Barrick, W. Stuart, and C. Krichbaum, 1970: *Radar Cross Section Handbook.* Vol. 2. Plenum Press, 949 pp.

Ryzhkov, A. V., and D. S. Zrnić, 1995: Precipitation and attenuation measurenents at a 10-cm wavelength. *J. Appl. Meteor.*, **34,** 2121–2134.

Ulaby, F. T., and M. C. Dobson, 1989: *Handbook of Radar Scattering Statistics for Terrain.* Artech House, 357 pp.

——, and J. J. van Zyl, 1990: Scattering matrix representation for simple targets. *Radar Polarimetry for Geoscience Applications,* F. T. Ulaby and C. Elachi, Eds., Artech House, 1–52.

——, T. E. Van Deventer, J. R. East, T. F. Haddock, and M. E. Coluzzi, 1988: Millimeter-wave bistatic scattering from the ground and vegetation targets. *IEEE Trans. Geosci. Remote Sens.*, **26,** 229–243.

Zahrai, A., and D. Zrnić, 1997: Implementation of polarimetric capability for the WSR-88D (NEXRAD) radar. Preprints, *28th Inter. Conf. on Radar Meteorology,* Austin, TX, Amer. Meteor. Soc., 284–285.

Zrnić, D. S., 1987: Three-body scattering produces precipitation signature of special diagnostic value. *Radio Sci.*, **22,** 76–86.

——, V. N. Bringi, N. Balakrishnan, K. Aydin, V. Chandrasekar, and J. Hubbert, 1993: Polarimetric measurements in severe hailstorm. *Mon. Wea. Rev.,* **121,** 2223–2238.

Unauthenticated | Downloaded 04/13/21 05:55 AM UTC